

Three-Dimensional Nucleic Acid Nanostructures Based on Self-Assembled Polymer-Oligonucleotide Conjugates of Comblike and Coil-Comb Chain Architectures

Erik Dimitrov, Natalia Toncheva-Moncheva,* Jordan A. Doumanov, Kirilka Mladenova, Svetla Petrova, Stergios Pispas, and Stanislav Rangelov*



Cite This: *Biomacromolecules* 2023, 24, 2213–2224



Read Online

ACCESS |



Metrics & More

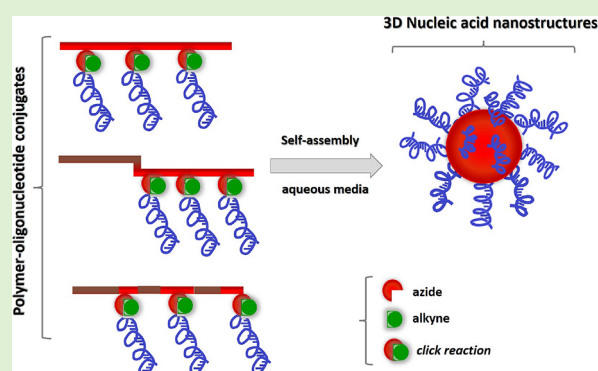


Article Recommendations



Supporting Information

ABSTRACT: Spherical nucleic acids have emerged as a class of nanostructures, exhibiting a wide variety of properties, distinctly different from those of linear nucleic acids, and a plethora of applications in therapeutics and diagnostics. Herein, we report on preparation of 3D nucleic acid nanostructures, prepared by self-assembly of polymer–oligonucleotide conjugates. The latter are obtained by grafting multiple alkyne-functionalized oligonucleotide strands onto azide-modified homo-, block, and random (co)polymers of chloromethylstyrene via initiator-free click coupling chemistry to form conjugates of comblike and coil-comb chain architectures. The resulting conjugates are amphiphilic and form stable nanosized supramolecular structures in aqueous solution. The nanoconstructs are thoroughly investigated and a number of physical characteristics, in particular, molar mass, size, aggregation number, zeta potential, material density, number of oligonucleotide strands per particle, grafting density, and their relation to hallmark properties of spherical nucleic acids – biocompatibility, resistance against DNase I, cellular uptake without the need for transfection agents – are determined.



INTRODUCTION

Most forms of nucleic acids rely on the hybridized duplex. This fundamental structural unit determines the overall shape of nucleic acids (linear duplex, circular duplex, supercoils, etc.) that are made naturally in living organisms through sequence selection and base-pairing interactions. Synthetic structures, often regarded to as DNA nanotechnology and origami, have been prepared using the recognition properties of DNA to assemble duplexes into rationally designed shapes.^{1–3} Nowadays, DNA nanotechnologies play a significant role in the regenerative medicine, life sciences, and biomedical field.^{4–6} Distinctly different from these forms of DNA are the spherical nucleic acids (SNAs). These are 3D nanostructures composed of dense, oriented spherical arrays of short oligonucleotides covalently attached to the surface of a nanoparticle, which can be inorganic, hollow, or organic.^{7–10} The dense 3D arrangement of the oligonucleotides imparts unique properties to SNAs. Due to their low toxicity, ability of functionalization, biodegradability, precise control over the size and morphology as well as resistance to nuclease degradation, enhanced biological stability, ability to overcome different biological barriers, and cellular uptake with no need for transfection agents,¹¹ they have great potential for development of vaccines, novel therapeutic and theranostic schemes, and bio-imaging tools as well as immunostimulation and immunomodula-

tion,^{12–16} cell transfection,^{17–20} and gene regulation materials.^{20–23}

SNAs have been prepared with a variety of core materials including inorganic compositions (Au, Ag, Pt, SiO₂, Fe₃O₄, quantum dots) as well as organic and polymeric compositions.^{9,24–29} Although introducing great versatility in the chemistry, structure, and properties of the SNAs, the latter are yet underexplored. They can be obtained by self-assembly of amphiphilic conjugates, prepared from a synthetic polymer covalently linked to a short oligonucleotide strand, into core-shell type micelles. Normally, the synthetic polymers are hydrophobic – polyesters such as poly(lactic-co-glycolic acid) and poly(*ε*-caprolactone),^{10,28–30} polyethers such as poly(ethoxyethyl glycidyl ether),¹⁰ and also diene and vinyl polymers such as polybutadiene³¹ and polystyrene,³² respectively – and build the core of the structures, whereas the nucleic acid strands form the shell. Most of the polymer-

Received: February 6, 2023

Revised: March 22, 2023

Published: April 4, 2023



oligonucleotide conjugates are of linear diblock and rarely of triblock,¹⁰ chain architecture, which poses some limitations to obtain structures with high enough density of nucleic acids on the nanoparticle surface, capable of exhibiting the typical/hallmark properties of SNAs. Zhang et al.²⁹ have recently described a synthetic approach that relies on grafting of multiple nucleic acid strands on a single polymer chain, thereby increasing the density of the nucleic acid layer of the resulting structures. As a hydrophobic polymer, these authors used commercially available poly(ϵ -caprolactone) extended with a short block of azide-functionalized poly(ϵ -caprolactone) on which the nucleic acid strands were grafted to obtain coil-comb chain architecture. Micelles, composed of a polystyrene core and mixed DNA/poly(*N*-isopropylacrylamide) (DNA/PNIPAM) shell, have recently been reported.³² These structures, obtained by co-assembly of linear polystyrene-*b*-DNA and polystyrene-*b*-PNIPAM diblock copolymers, have been developed and optimized with regard to general SNA properties, which can be reversibly turned on and off employing the temperature sensitivity of PNIPAM, whereas the biologically inert polystyrene core was used as a scaffold for assembling and arranging of the mixed DNA/PNIPAM corona.

Herein, we report on the synthesis of novel amphiphilic polymer–oligonucleotide conjugates of comblike and coil-comb chain architectures and their self-assembly into 3D nucleic acid nanostructures. The polymers are based on homopolychloromethylstyrene and its random and block copolymers with polystyrene. They were converted into clickable entities to which appropriately functionalized single-stranded DNA oligonucleotides (ssODN) were grafted using metal-free click reactions. The self-assembly of the resulting conjugates was investigated emphasizing on the characterization of the particles and determination of parameters/characteristics such as molar mass, aggregation number, number of ssODN strands per particle, grafting density, etc. Preliminary biological evaluation of the 3D nucleic acid nanostructures was carried out as well.

EXPERIMENTAL SECTION

Materials. 1-Phenyl-1-(2,2,6,6-tetramethyl-1-piperidinyloxy)ethane (>98%, Sigma-Aldrich), *p*-chloromethylstyrene (CMS, >90% Sigma Aldrich), acetic anhydride (Ac2O, ReagentPlus, ≥99%, Sigma Aldrich), styrene (stabilized for synthesis Sigma-Aldrich), sodium azide (ReagentPlus, ≥99.5%, Sigma-Aldrich), and magnesium sulfate (anhydrous, ReagentPlus, ≥99.5%, Sigma-Aldrich) were used as received. Methylene chloride (>99.98%, Fisher Scientific) was dried with calcium hydride and freshly distilled before use. *N,N*-Dimethylformamide, (DMF, ACS reagent, ≥99.8%) and dimethyl sulfoxide (DMSO, ACS reagent, ≥99.9%) were dried by molecular sieves. Tetrahydrofuran (>99.5%, Fisher Scientific) was dried using calcium hydride and freshly distilled before use. Dibenzocyclooctyne-functionalized single-stranded DNA oligonucleotide (DBCO-ssODN) was purchased from Biomers.net GmbH. The sequences and composition of the oligonucleotide as well as a MALDI spectrum and a HPLC chromatogram are shown in the SI (Table S1 and Figure S1). Deionized water was obtained by a Millipore MilliQ system and was additionally filtered through a 220 nm PTFE filter and a 20 nm cellulose filter.

Synthesis of Polychloromethylstyrene (co)Polymers. Polychloromethylstyrene homopolymer (PCMS), polychloromethylstyrene-*b*-polystyrene block copolymer (PCMS-*b*-PS), and poly(chloromethylstyrene-*ran*-styrene) random copolymer (P(CMS-*ran*-S)) were synthesized by nitroxide-mediated controlled radical polymerization.³³ In brief, the reactions took place in vacuum-sealed glass ampules, while the resulting polymers were recovered after three

freeze–thaw cycles and heating in an oil bath for 4 h at 125 °C. For the synthesis of PCMS, 1-phenyl-1-(2,2,6,6-tetramethyl-1-piperidinyloxy)ethane (unimolecular initiator) and *p*-chloromethylstyrene (CMS) were used, with acetic anhydride as an accelerator. In the case of PCMS-*b*-PS, PCMS was dissolved in styrene and acetic anhydride before the polymerization reaction of styrene to form the PS block took place. For the synthesis of the random P(CMS-*ran*-S) copolymer, styrene and CMS were copolymerized with 1-phenyl-1-(2,2,6,6-tetramethyl-1-piperidinyloxy)ethane and acetic anhydride. The molar mass characteristics and composition of the (co)polymers are shown in Table 1.

Table 1. Characterization Data of the PCMS Homopolymer, PCMS-*b*-PS Block, and P(CMS-*ran*-S) Random Copolymers

sample code	M_w^{SEC} (g mol ⁻¹)	M_w/M_n^{SEC}	wt % (PCMS)	wt % (PS)
PCMS	11,000	1.45	100 (72 units)	0 (0 units)
P(CMS- <i>ran</i> -S)	10,000	1.28	30 (20 units)	70 (68 units)
PCMS- <i>b</i> -PS	16,500	1.14	11 (12 units)	89 (142 units)

Functionalization of PCMS, PCMS-*b*-PS, and P(CMS-*ran*-S). 0.1195 g (0.0108 mmol, 1 equiv) of PCMS, 0.1111 g (0.006736 mmol, 1 equiv) of PCMS-*b*-PS, and 0.09334 g (0.009334 mmol, 1 equiv) of P(CMS-*ran*-S) were dissolved separately in 15 mL of DMF and 0.5084 g (7.8218 mmol, 720 equiv), 0.0517 g (0.8083, 120 equiv), and 0.1213 g (1.8668 mmol, 200 equiv), respectively, of NaN₃ were added to the solutions. The mixtures were stirred at room temperature for 24 h and after that poured in 70 mL of water. The solutions were extracted 3 times with 30 mL of methylene chloride. The combined extracts were dried with anhydrous MgSO₄ and concentrated to about 50 mL. Evaporation of the solvent gave 110.6 mg of poly(azidomethylstyrene) (PN₃MS), 93% yield, 111.0 mg of polyazidomethylstyrene-*b*-polystyrene (PN₃MS-*b*-PS), 99% yield, and 92.0 mg of poly(azidomethylstyrene-*ran*-styrene) (P(N₃MS-*ran*-S)), 98% yield.

Synthesis of Polymer-Oligonucleotide Conjugates of Comblike Chain Architecture. DBCO-ssODN (766.6 μg, 110 nmol, 5 equiv) was dissolved in 2.0 mL of a dry solvent mixture (DMSO/DMF, v/v 1/1) and placed in a round-bottom flask under an argon atmosphere. The solution was purged with argon and stirred vigorously for 20 min. Separately, the PN₃MS homopolymer (242 mg, 21.99 nmol, 1 equiv) was dried by azeotropic distillation in toluene. The dry product was dissolved in 0.5 mL of a dry solvent mixture (DMSO/DMF, v/v 1/1) and added via a syringe to the DBCO-ssODN solution. The azide–alkyne click coupling reaction was carried out under argon at 40 °C for 24 h. The reaction mixture was cooled to room temperature and purified by intense dialysis against the DMSO/DMF mixture for 2 days, using dialysis tubes with a molecular weight cutoff (MWCO) of 15 kDa membrane. Yield: 765 μg, 99.7%. The conjugate is denoted ssODNconjH.

Similarly, DBCO-ssODN (766.6 μg, 110 nmol, 5 equiv) was dissolved in 2.0 mL of a dry solvent mixture (DMSO/DMF, v/v 1/1) and placed in a round-bottom flask under argon atmosphere. The solution was purged with argon and stirred vigorously for 20 min. Separately, P(N₃MS-*ran*-S) random copolymer (242 μg, 21.99 nmol, 1 equiv) was dried by azeotropic distillation in toluene. The dry product was dissolved in 0.5 mL of a dry solvent mixture (DMSO/DMF, v/v 1/1) and added via a syringe to the DBCO-ssODN solution. The azide–alkyne click coupling reaction was carried out under argon at 40 °C for 24 h. The reaction mixture was cooled to room temperature and purified following the procedure described above. Yield: 725 μg, 94.6%. The conjugate is denoted ssODNconjR.

Synthesis of Polymer-Oligonucleotide Conjugate of Coil-Comb Chain Architecture. DBCO-ssODN (766.6 μg, 110 nmol, 8 equiv) was dissolved in 2.0 mL of a dry solvent mixture (DMSO/DMF, v/v 1/1) and placed in a round-bottom flask under argon atmosphere. The solution was purged with argon and stirred

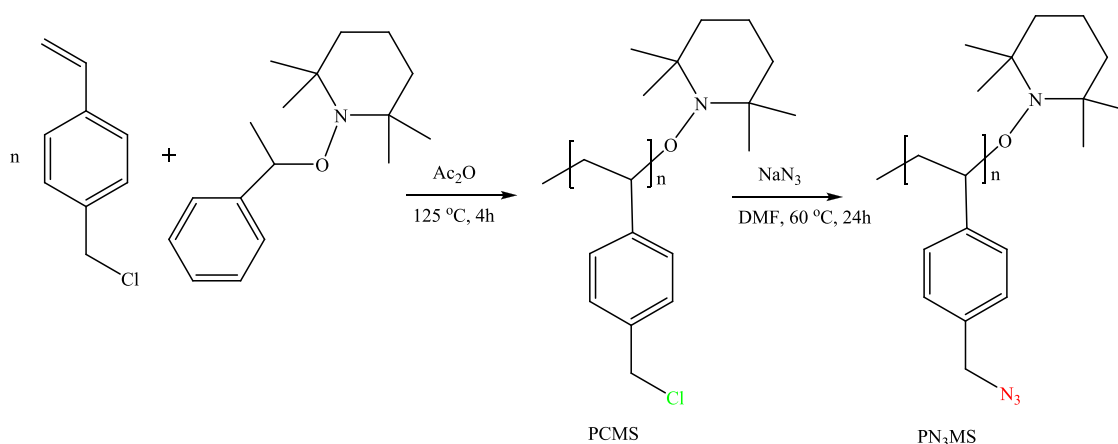


Figure 1. Synthesis of the initial PCMS homopolymer and the functionalized intermediate PN₃MS homopolymer.

vigorously for 20 min. Separately, PN₃MS-*b*-PS block copolymer (227.7 mg, 13.79 nmol, 1 equiv) was dried by azeotropic distillation in toluene. The dry product was dissolved in 0.5 mL of a dry solvent mixture (DMSO/DMF, v/v 1/1) and added via a syringe to the DBCO-ssODN solution. The azide–alkyne click coupling reaction was carried out under argon at 40 °C for 24 h. The reaction mixture was cooled to room temperature and purified following the procedure described above. Yield: 690 μg, 90.0%. The conjugate is denoted ssODNconjB.

Preparation of Nanoparticles by Self-Assembly of ssODNconjH, ssODNconjR, and ssODNconjB. Nanoparticles were obtained by the solvent displacement method. Solutions of ssODNconjH, ssODNconjR, and ssODNconjB in DMSO/DMF were dialyzed against ultrapure MilliQ water for 3 days and then purified by ultrafiltration, which yielded a colorless slightly opalescent aqueous dispersion of ssODNconjH, ssODNconjR, and ssODNconjB nanoparticles.

METHODS

Size Exclusion Chromatography (SEC). Analyses were performed on a Shimadzu Nexera HPLC chromatograph, equipped with a degasser, a pump, an auto-sampler, an RI detector, and three columns: 10 μm PL gel mixed-B, 5 μm PL gel 500 and 50 Å. Tetrahydrofuran was used as the eluent at a flow rate of 1.0 mL min⁻¹ and temperature of 40 °C. The sample concentration was 1 mg mL⁻¹, and SEC was calibrated with polystyrene standards.

Nuclear Magnetic Resonance (¹H NMR). ¹H NMR measurements were conducted on a Bruker Avance II spectrometer operating at 600 MHz using CDCl₃ as the solvent at 25 °C.

Light Scattering. Dynamic light scattering (DLS) measurements were performed on a Brookhaven BI-200 goniometer with vertically polarized incident light at a wavelength λ = 633 nm supplied by a He–Ne laser operating at 35 mW and equipped with a Brookhaven BI-9000 AT digital autocorrelator. The scattered light was measured for dilute aqueous dispersions of ssODNconjH, ssODNconjR, or ssODNconjB nanoparticles in the concentration range 0.0186–0.05991 mg·mL⁻¹ at 25 °C. Measurements were made at angles θ in the range of 50–130°. The autocorrelation functions were analyzed using the constrained regularization algorithm CONTIN³⁴ to obtain the distributions of the relaxation rates (Γ). The latter provided distributions of the apparent diffusion coefficient ($D = \Gamma/q^2$), where q is the magnitude of the scattering vector given by $q = (4\pi n/\lambda)\sin(\theta/2)$ where n is the refractive index of the medium. The mean hydrodynamic radius was obtained by the Stokes–Einstein eq 1:

$$R_h = kT/(6\pi\eta D_0) \quad (1)$$

where k is the Boltzmann constant, η is the solvent viscosity at temperature T in Kelvin, and D_0 is the diffusion coefficient at infinite dilution.

Static light scattering (SLS) measurements were carried out in the interval of angles from 40 to 140° at 25 °C using the same light scattering set. The SLS data were analyzed using the Berry plot software provided by Brookhaven Instruments. Information on the weight-average molar mass, M_w , the radius of gyration, R_g , and the second virial coefficient, A_2 , was obtained from the dependence of the quantity $(Kc/R_\theta)^{1/2}$ on the concentration (c) and scattering angle (θ). Here, K is the optical constant given by $K = 4\pi^2 n_0^2 (dn/dc)^2 / N_A \lambda^4$, where n_0 is the refractive index of the solvent, N_A is Avogadro's constant, λ is the laser wavelength, and R_θ is the Rayleigh ratio at angle θ . dn/dc is the refractive index increment measured in water in separate experiments on an Orange GPC19 DNDC refractometer. The dn/dc values of the investigated systems were in the 0.139–0.142 mL g⁻¹ range.

The electrophoretic light scattering measurements were carried out on a 90Plus PALS instrument (Brookhaven Instruments Corporation) equipped with a 35 mW red diode laser ($\lambda = 640$ nm) at a scattering angle (θ) of 15°. ζ potentials were calculated from the obtained electrophoretic mobility at 25 °C by using the Smoluchowski eq 2:

$$\zeta = 4\pi\eta v/\epsilon \quad (2)$$

where η is the solvent viscosity, v is the electrophoretic mobility, and ϵ is the dielectric constant of the solvent.

Gel Electrophoresis. Gels containing 1% agarose (w/w) were run on an FBSB-710 electrophoresis unit (Fisher Biotech) in 1 × Tris-Borate EDTA (TBE) buffer at room temperature and 60 V. Imaging was carried out by ethidium bromide staining and UV illumination (302 nm). The gels were imaged using a gel reader Alpha Innotech.

Cell Cultures. A549 (human lung carcinoma) cells were grown in DMEM with 10% (v/v) FCS, streptomycin (0.1 mg mL⁻¹), penicillin (0.06 mg mL⁻¹) at 37 °C in a 5% CO₂ water-saturated atmosphere.

MTT Assay. Metabolic activity of A549 cells was assessed using the MTT assay. The cells with an initial concentration of 1×10^4 cells per well were grown on 96-well plates for 24 h and were incubated for 6 h with ssODNconjH, ssODNconjR, or ssODNconjB nanoparticles in different concentrations: 0.02, 0.05, 0.08, 0.10, 0.12, and 0.15 μM. The MTT assay was performed after treatment with ssODNconjH, ssODNconjR, or ssODNconjB nanoparticles. Untreated cells were used as a control.

Fluorescence Microscopic Imaging. A549 cells (1×10^5) per well were seeded in 24-well plates for 24 h at 37 °C before treatment with ssODNconjH nanoparticles containing 0.2% of DPH ($\lambda_{ex} = 353$ nm; $\lambda_{em} = 430$ nm). The cells were incubated with ssODNconjH nanoparticles at a concentration of 0.8 μM per well for 30 min, and immediately after treatment, the nanoparticles in live cells were visualized by a fluorescent microscope (GE Delta Vision Ultra Microscopy System).

DNase Activity Assay. Endonuclease activity of DNase I (EC 3.1.21.1) on the ssODNconjH, ssODNconjR, or ssODNconjB nanoparticles was assayed using the manufacturers' instructions and

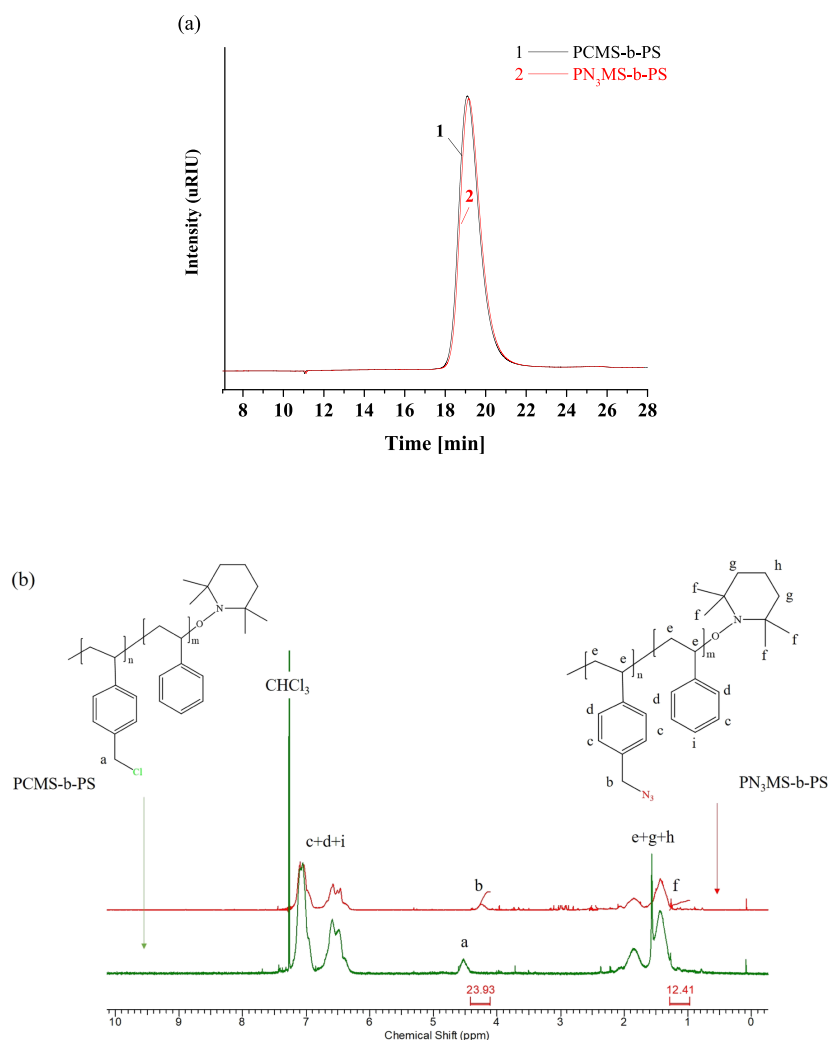


Figure 2. SEC curves (a) and ¹H NMR spectra (b) of the initial PCMS-*b*-PS block copolymer and the functionalized intermediate PN₃MS-*b*-PS block copolymer in CDCl₃. The integrals of the methyl protons of TEMPO (protons *f*) and methylene protons from CH₂N₃ groups of PN₃MS moieties (protons *b*) are shown.

compared with DNase I activity on free oligonucleotides as described elsewhere.¹⁰ One enzyme unit was defined as the amount of DNase I added to 1 mg mL⁻¹ oligonucleotides that will produce ΔA₂₆₀ of 0.001 at 260 nm per min per mL when assayed in a 0.1 M NaOAc (pH 5.0) buffer, containing 4.2 mM magnesium sulfate and 25 mM sodium chloride.

RESULTS AND DISCUSSION

Synthesis and Characterization of Polymer–Oligonucleotide Conjugates. To develop SNAs with organic/polymeric cores stabilized by a shell of nucleic acid strands of high density, we designed a series of polymer–oligonucleotide conjugates of comblike and coil-comb chain architectures. The latter were prepared by grafting multiple single-stranded DNA oligonucleotide (ssODN) strands onto homo- and random and block (co)polymers. The synthetic approach is based on a click coupling reaction of monofunctionalized ssODN with appropriately functionalized synthetic (co)polymers. First, the polychloromethylstyrene (PCMS) homopolymer and also block (PCMS-*b*-PS) and random P(CMS-*ran*-S) copolymers of styrene and chloromethylstyrene were prepared by nitroxide-mediated controlled radical polymerization (Figure 1, Figure S2 in the SI) as described elsewhere.³³ The molar mass characteristics and composition of the starting (co)polymers

are presented in Table 1. Next, by treatment of the (co)polymers with sodium azide in DMF at 60 °C overnight, the pendant chlorides were converted into azides (Figure 1, Figure S2 in the SI) to prepare polyazidomethylstyrene (co)polymers – PN₃MS homopolymer and block, PN₃MS-*b*-PS, and random, P(N₃MS-*ran*-S) copolymers.

Size exclusion chromatography (SEC) and proton nuclear magnetic resonance (¹H NMR) analyses were used to characterize the products. SEC (Figure 2a, Figure S3 in the SI) of the starting PCMS (co)polymers revealed monomodal, mainly symmetric peaks with molecular weight distributions (Table 1) consistent with what is typically observed for nitroxide-mediated controlled radical polymerization.³⁵ Upon substituting with N₃ groups, the functionalized PN₃MS (co)polymers exhibited no changes in the retention time and the SEC curves of the initial and functionalized (co)polymers fully overlapped (Figure 2a, Figure S3), indicating that undesirable side reactions (e.g., degradation) did not take place.

The successful and complete azidation was proven by ¹H NMR (Figure 2b, Figure S4), where, together with all characteristic signals assigned for the structures of PCMS, PCMS-*b*-PS, and P(CMS-*ran*-S), a new signal at 4.25 ppm

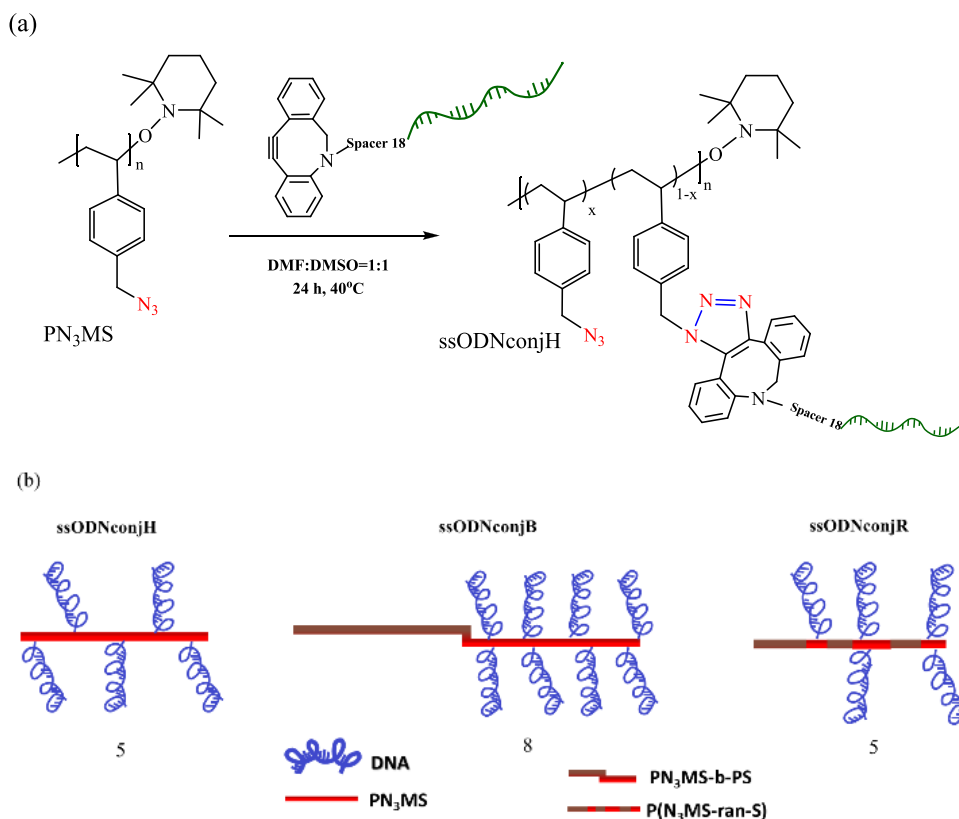


Figure 3. (a) Schematic presentation of the synthesis of the polymer–oligonucleotide conjugate, ssODNconjH, by copper-free click reaction of PN₃MS homopolymer and dibenzocyclooctyne-functionalized ssODN. (b) Chain architecture of the polymer–oligonucleotide conjugates ssODNconjH, ssODNconjR, and ssODNconjB. Numbers below the structures indicate the average number of oligonucleotide strands per (co)polymer chain.

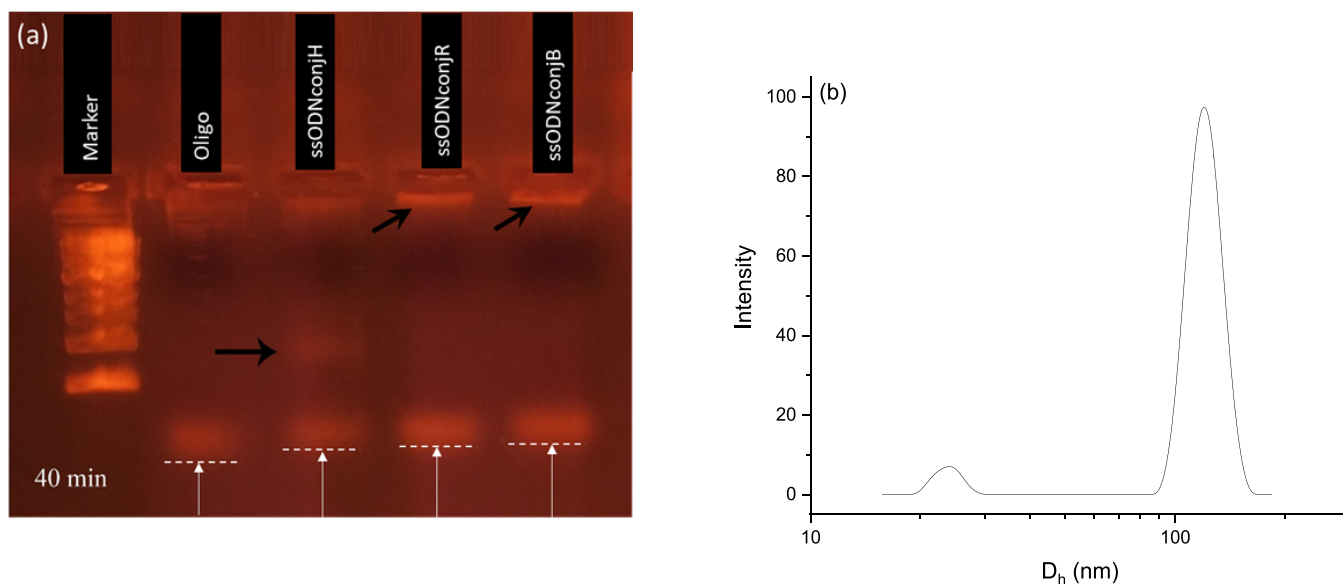


Figure 4. (a) Agarose gel retardation patterns of dibenzocyclooctyne-functionalized oligonucleotide and ssODNconjH, ssODNconjR, and ssODNconjB. The white arrows indicate the different retardations of the pure dibenzocyclooctyne–oligonucleotide and conjugates. The black arrows indicate appearance of bands associated with formation of a second fraction of supramolecular particles. Nucleic acids were stained with ethidium bromide. Overall duration of the experiment was 40 min. (b) Particle size distribution from DLS, measured at an angle of $\theta = 90^\circ$ for aqueous dispersion of ssODNconjB at concentration $c = 0.010 \text{ mg mL}^{-1}$ and 25 °C.

corresponding to methylene protons adjacent to the azide group appeared, while the signal at 4.52 ppm assigned to methylene protons next to the pendant chlorides completely disappeared (Figure 2b and Figure S4). In addition, the

integral ratios of the signals from the methyl protons of TEMPO at 1.1 ppm and methylene protons of CH₂N₃ groups at 4.25 ppm for PN₃MS-b-PS (12/24, corresponding to 24 protons, that is, 12 units, see Figure 2b and Table 1), PN₃MS

(12/140, corresponding to 140 protons, that is 70 units, see Figure S4a and Table 1), and P(N₃MS-*ran*-S) (12/40, corresponding to 40 protons, that is 20 units, see Figure S4b and Table 1) were almost equal to the theoretical values, indicating that the azidation proceeded quantitatively.

In the final step, ssODN strands were grafted onto the (co)polymer chains by an azide–alkyne click reaction as presented in Figure 3a and Figure S5. Proper amounts of dibenzocyclooctyne-functionalized ssODN were added to the azidated (co)polymers in an organic solvent mixture to initiate the reaction. Given the strain of the alkyne ring, the reaction smoothly proceeds as a strain-promoted cycloaddition without the need for catalysts/catalytic complexes. The amounts of dibenzocyclooctyne-functionalized ssODN were in 5 to 8-fold molar excess, whereas, with regard to the azido groups, they were in deficiency. This implied that several ssODN strands would be attached to each (co)polymer chain and, at the same time, a number of azido groups and hence azidomethylstyrene units would remain unreacted.

Upon completion of the conjugation reactions, the products were purified by dialysis against the mixed DMSO/DMF solvent with a MWCO of 8 kDa membrane to remove the unreacted dibenzocyclooctyne-functionalized ssODN and replacement of the organic solvents with ultrapure MilliQ water followed by ultrafiltration. In any case, precipitates were not formed and the yields were close to the theoretical ones (90.0–99.7%), implying that the click reactions proceeded quantitatively and all reactants were converted into products. By measuring the absorbance of the aqueous solutions at 260 nm (Figure S6 in the SI) and based on the total yields of the products, it was determined that an average of 5, 5, and 8 ssODN strands were conjugated onto each polymer chain of the PN₃MS homopolymer, random P(N₃MS-*ran*-S) copolymer, and block PN₃MS-*b*-PS copolymer, respectively (see the SI). Schematic presentation of the chain architecture of the conjugates, the introduced abbreviations, and the average number of oligonucleotide strands per (co)polymer chain are shown in Figure 3b.

Aqueous Solution Properties. Agarose gel electrophoresis was used to analyze the resulting conjugates (Figure 4a). Consistent with the enlargement of the molar mass, the electrophoretic mobility of the conjugates was retarded compared to that of dibenzocyclooctyne-functionalized oligonucleotide, used as control (white arrows, Figure 4a). In the investigated concentration range (around 10 μg mL⁻¹), additional bands were clearly observed (black arrows, Figure 4a), indicating formation of a second fraction of particles significantly larger in size and/or different in charge, compared to those responsible for the major bands. This observation was corroborated by DLS. Figure 4b shows a particle size distribution typically observable in the above concentration range. The low amplitude fast mode is associated with particles of hydrodynamic radii of about 10 nm, identified as unimers, that is, non-associated macromolecules of the conjugates, whereas the dominant peak corresponded to considerably larger particles (tens of nanometers) – presumably multichain aggregates.

Upon increasing concentration, the fast mode gradually disappeared and monomodal size distribution was manifested (Figure 5a). Multiangle static and dynamic light scattering was performed in the concentration range 0.0186–0.05991 mg·mL⁻¹ in order to determine the fundamental structural parameters of the aggregates. The diffusion coefficients, *D*, of

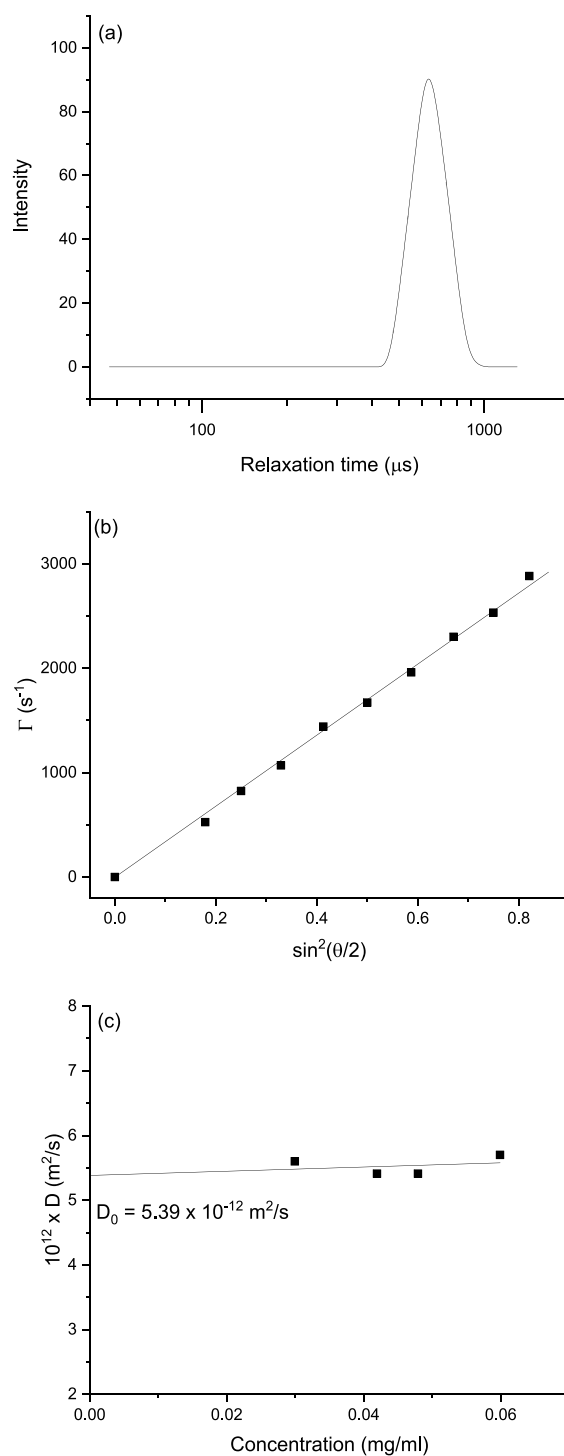


Figure 5. (a) Representative relaxation time distribution (τ) measured at an angle of 90° for aqueous dispersion of ssODNconjR at a concentration of 0.0372 mg mL⁻¹. (b) Relaxation rate (Γ) as a function of $\sin^2(\theta/2)$ for ssODNconjR at concentration of 0.0186 mg mL⁻¹. (c) Concentration dependence of the diffusion coefficients for ssODNconjH. The lines through the data points in panels (b) and (c) represent the linear fit to the data. Measurements were performed at 25 °C.

the aggregates in aqueous solution were determined from the slopes of the angular dependences of the relaxation rate, Γ , as shown in Figure 5b and then plotted against concentration to obtain the values of the diffusion coefficient at infinite dilution,

Table 2. Static, Dynamic, and Electrophoretic Light Scattering Characterization Data of Aggregates Formed by the Conjugates in Aqueous Solution^a

conjugate	$10^{-6} \times M_w$ (g/mol)	R_g (nm)	$10^5 \times A_2$ (mL mol g ⁻²)	R_h (nm)	R_g/R_h	ρ (mg mL ⁻¹)	ζ (mV)	N_{agg}	$N_{s/p}$	σ (nm ⁻²)
ssODNconjH	16.8	40.6	-4.0	45.5	0.89	70.7	-17.9	367	1835	0.071
ssODNconjR	25.8	41.1	0.7	48.1	0.85	91.9	-16.8	577	2885	0.099
ssODNconjB	37.8	51.2	2.1	49.7	1.03	122.1	-15.6	524	4192	0.135

^a ρ , N_{agg} , $N_{s/p}$, and σ denote the density of the material within the particle, aggregation number, number of oligonucleotide strands per particle, and grafting density, respectively. The standard deviations are up to 4% for static and dynamic light scattering parameters and 3% for the ζ potential.

D_0 (Figure 5c). The latter were used to calculate the hydrodynamic radii, R_h . The values of R_h are collected in Table 2. They are in the 45–50 nm range being largest for the aggregates of the conjugate derived from the block copolymer.

The Berry plot method was used to determine the static light scattering parameters – weight-average molar mass (M_w), second virial coefficient (A_2), and radius of gyration (R_g). A representative Berry plot is shown in Figure 6. All parameters

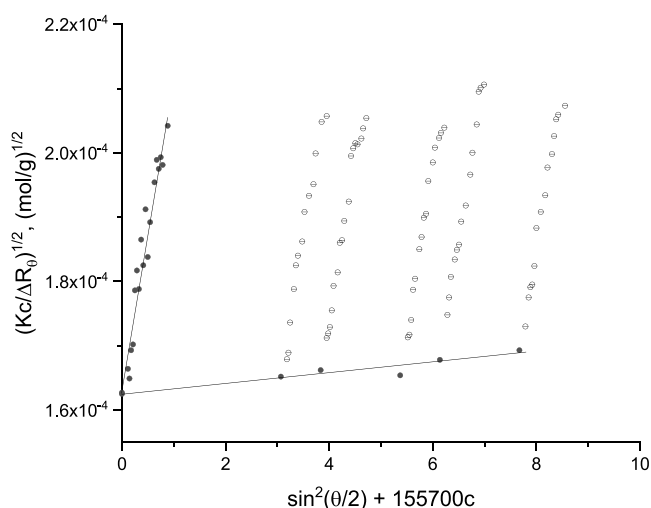


Figure 6. Berry plot of ssODNconjB in aqueous solution. Open symbols and closed symbols represent experimental points and extrapolated points to zero concentration and zero angle, respectively. Measurements were performed at 25 °C.

derived from static light scattering measurements are collected in Table 2. Furthermore, the aggregation number (N_{agg}) was calculated using molar mass data from Table 2 and nominal molar masses of the corresponding conjugates.

In contrast to the aggregates of other nucleic acid–polymer conjugates differing in chain architecture, composition, and oligonucleotide content,¹⁰ the molar masses of the aggregates of the present conjugates were found to increase in the order ssODNconjH – ssODNconjR – ssODNconjB (Table 2). This

can be attributed to the enhancement of the hydrophobicity of the conjugates by introducing styrene units (ssODNconjR) and/or their arrangement in blocks (ssODNconjB), where segregation of polystyrene blocks is favored; see also Figure 3b. The values of A_2 are generally low in magnitude ($\sim 10^{-5}$), which is consistent with the high molar masses. The negative value of A_2 for ssODNconjH, apparently indicating unfavorable particle–solvent interactions, might be somewhat surprising at first sight but can be related to the lowest both number of oligonucleotide strands per particle, $N_{s/p}$, and surface density, σ (Table 2). The variations of R_g followed those of R_h , however, in somewhat a wider range, which was reflected by the R_g/R_h ratio (Table 2). The latter was found to vary in an interval (0.85–1.03), which was slightly above the theoretical value for hard spheres of 0.775,^{36,37} implying formation of relatively compact and dense particles with “hairy” surface.^{36,38}

A more realistic assessment of how compact the particles are can be given by the density of the material within the particle, ρ . This quantity was calculated from the molar mass and hydrodynamic volume data assuming spherical morphology of the particles (see the SI for the calculation of ρ). The resulting values, listed in Table 2, ranged in the 70.0–122.1 mg mL⁻¹ interval and were compatible with, though being slightly lower than, the familiar block copolymer micelles in aqueous solution.^{39–43} Apparently, ρ is dependent on the content of styrene units: while the ssODNconjB aggregates were characterized with the highest density due to the highest content of styrene units (Table 1) with the important contribution of being arranged in a polystyrene block that is truly hydrophobic, the aggregates of ssODNconjH (no styrene units) were considerably less compact and dense. ssODNconjR takes an intermediate position between these two extremes.

$N_{s/p}$ was given by the product of N_{agg} and the average number of oligonucleotide strands conjugated to each polymer chain of the homopolymer, random and block copolymers. Typical values for reference SNAs^{44–47} vary between 70 and 1200 strands per particle though considerably larger values have recently been reported.^{10,27,48,49} Consistent with their relatively large dimensions and comblike and coil-comb chain architectures of the conjugates comprising 5–8 oligonucleotide

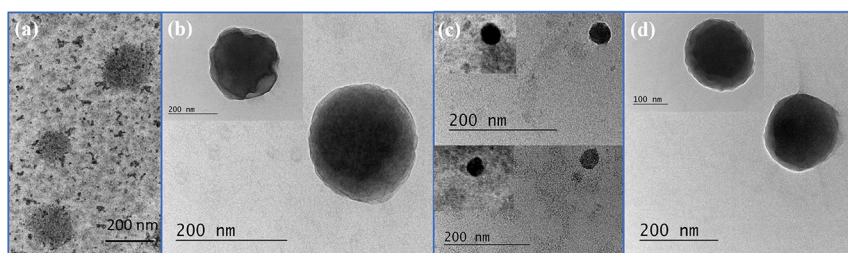


Figure 7. Representative TEM images of polymer–oligonucleotide conjugates ssODNconjH (panels a and b), ssODNconjR (panel c), and ssODNconjB (panel d) nanoparticles, formed in aqueous solution.

strands per polymer chain, $N_{s/p}$ values of the present aggregates are larger than those of reference SNAs.^{44–47} $N_{s/p}$ went through a maximum for ssODNconjB apparently owing to the highest oligonucleotide content (8 strands per polymer chain). The aggregates exhibited moderately negative ζ potentials due to the negative charge of the grafted ssDNA strands, without any pronounced trend that could be associated with the variations of e.g., size, N_{agg} or $N_{s/p}$.

Transmission electron microscopy (TEM) was performed to resolve the morphology of the structures. In all cases, the spherical morphology of the particles was readily apparent (Figure 7). The objects were well-separated with dimensions in the dry state that were apparently consistent with the results from DLS, which implied that they did not contain much water.

The grafting density and the conformation of the oligonucleotide strands represent aspects to be considered since the unique properties of the SNAs stem from the density and orientation of the nucleic acid strands in the outer region of the nanoconstructs. The grafting density was calculated from $N_{s/p}$ and hydrodynamic dimensions of the particles assuming that (i) the particles were spherical in shape and (ii) all strands were located in the shell of the assemblies (see the SI for the calculation of σ). σ is expressed as the number of strands per nm^2 and the values are collected in Table 2. As evident from Table 2, σ ranged in an interval from 0.071 to 0.135 nm^{-2} , which is compatible with that of reference SNAs structures.^{29,47,48,50,51} Consistent with the highest $N_{s/p}$, σ attained the highest value for the aggregates of ssODNconjB.

In no case, however, were the oligonucleotide strands in the brush regime. Indeed, regarding the strands as surface-anchored random coils, the transition to fully extended conformation and brush regime can be determined by $\sigma_{tr} = 1/R_F^2$,⁵² where R_F is the Flory radius. Considering the composition of the oligonucleotide, values of 2.54 nm and 0.155 nm^{-2} were obtained for R_F and σ_{tr} , respectively (see the SI for the calculation of R_F and σ_{tr}). Since the grafting density of the investigated systems was invariably lower than σ_{tr} , one may conclude that the oligonucleotide strands did not enter the fully extended, brush regime. It is noteworthy that none of the SNA constructs that have been previously reported exhibit grafting density values larger than σ_{tr} ,⁴⁸ implying that adopting a brush conformation is not a prerequisite to manifest the typical SNA properties.

Biological Evaluation. The aggregates exhibited remarkable colloidal stability for at least 2 months at 4°C and sterile conditions, which can be attributed to the formation of a shell by ordering oligonucleotides into a dense, spherical spatial arrangement. Such arrangement can also provide the structures with other properties such as low toxicity, improved nuclease stability, and ability to cross cell membranes without the need for transfection agents.^{8,16,20,29,50} The biological relevance in terms of cellular toxicity, resistance to enzymatic degradation, and cell internalization of the structures, that the present polymer–oligonucleotide conjugates formed was evaluated.

The MTT assay was performed using A549 (human lung carcinoma) cells. The metabolic activity was determined after 6 h of incubation of the cells with the nanoparticles of ssODNconjH, ssODNconjR, and ssODNconjB in a concentration dependent manner. The treatment of A549 eukaryotic cells with the nanoparticles caused biologically significant changes in metabolic activity and viability. The nanoparticles displayed no cytotoxic effect for all used concentrations, and an

increased metabolic activity by ca. 25% compared to the untreated control cells was observed (Figure 8). The uptake of

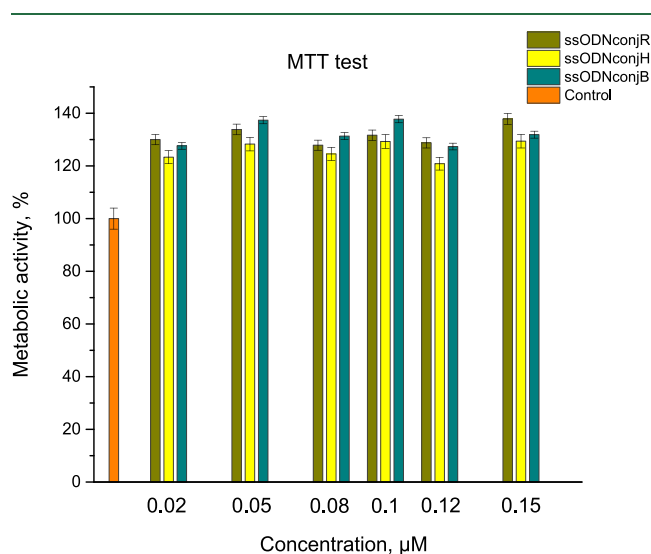


Figure 8. Metabolic activity of A549 cells after 6 h of incubation with different nanoparticles of ssODNconjH, ssODNconjR, and ssODNconjB in the concentration range indicated. The MTT analysis was performed immediately after the sixth hour of nanoparticle treatment. Each data point represents the arithmetic mean \pm SD of 7 separate experiments run in triplicate. Metabolic activity is presented as a percent of untreated control cells.

hydrophilic nanoparticles, consisting of biodegradable oligonucleotides, and the altered levels of exo- and endocytosis of molecules distinct to the cells are always associated with changes of cell sensing, signaling, and metabolic activities of the cells.^{10,53} The change of metabolic activity of A549 cells is the proof that the cells react to nanoparticles.

The enhanced nuclease stability of the SNA structures is typically associated with reduced exposure of the nucleic acid strands to nucleases.^{16,20} In that aspect, enhancement of the resistance to nuclease degradation with increasing grafting density due to steric hindrance can be anticipated. The stability of the ssODNconjH, ssODNconjR, and ssODNconjB aggregates was tested against DNase I endonuclease (Figure 9). Reduction of the enzyme specific activity compared to the control unmodified oligonucleotide of the same number of bases was observed for all tested SNA structures. It was significant – above 90% – for the aggregates of ssODNconjB and ssODNconjR, which are characterized with the highest grafting density of the nucleic acid strands (Table 2). The less dense shell of the ssODNconjH aggregates probably allowed enhanced access of the nuclease to the oligonucleotide strands and therefore the endonuclease activity was reduced by ca. 15% only. Contribution to the lowering of the enzyme activity reduction may have also the less compact and loose structure of ssODNconjH aggregates (see above density of the material within the particle, Table 2).

The most intriguing and valuable property of the SNAs is their ability to enter cells in high quantity without a carrier system.⁸ It has been commonly accepted that SNA internalization occurs via scavenger-mediated endocytosis.⁵⁴ Scavenger receptors are cell surface receptors that are capable of recognizing and taking up macromolecules having negative charge density.⁵⁵ To examine this property, A549 cells were incubated with ssODNconjH aggregates, loaded with 1,6-

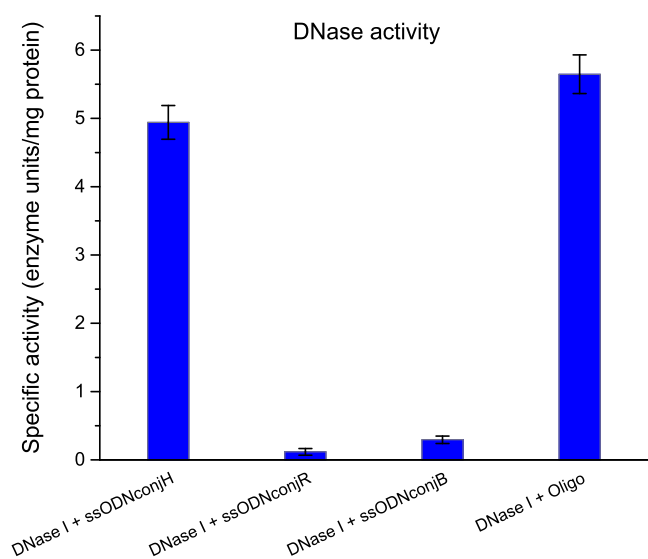


Figure 9. DNase I enzyme specific activity against aggregates of ssODNconjH, ssODNconjR, and ssODNconjB. Control: unmodified oligonucleotide of the same number of bases.

diphenyl-1,3,5-hexatriene (DPH). DPH is a fluorescent dye, which is sparingly soluble and non-fluorescent in water, but in a hydrophobic environment exhibits a strong increase in fluorescence. DPH is widely used in studies of bilayer membrane interiors and fluidity,^{56,57} for determination of critical micellization concentrations of surfactants and polymer amphiphiles, and detecting of hydrophobic domains in (polymeric) micelles and nanoparticles.^{41,58–63} For this experiment, the aggregates of ssODNconjH were purposefully selected due to their less compact and dense structure exhibiting the lowest material density within the particle (Table 2). Such a loose structure would facilitate the penetration of the DPH molecules in the interior of the particles hopefully without disturbing their initial genuine structural arrangement. Labeled with DPH, ssODNconjH aggregates entered A549 cells readily after 30 min incubation (Figure 10). Their ability to cross the cell membrane without

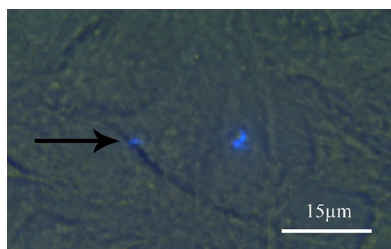


Figure 10. Fluorescence micrographs of A549 cells following 30 min exposure to ssODNconjH aggregates. The particles taken up by the cells are indicated by arrows. Scale bar represents 15 μm .

the assistance of cationic transfection agents is noteworthy. After internalization, the negatively charged ssODNconjH aggregates were observed as small granules, denoted by arrows in Figure 10.

As A549 cells normally take up nanoparticles via caveolin-mediated pathways, the common route of the internalized nanoparticles is maturing in the late endosomes and degradation in the lysosomes.⁶⁴ Nanoparticles, however, could bypass the lysosomal degradation and deliver their

cargo to various cellular destinations including cytosol, endoplasmic reticulum, Golgi apparatus, mitochondria, even nucleus. In that aspect, the non-covalent architecture and dynamic structure of the aggregates of the present conjugates is beneficial since it could lead to release of intact macromolecules bearing oligonucleotides that, due to their smaller size and molar mass, could reach and enter nucleus. In the context of antisense regulation of long encoding RNAs, Sprangers et al.⁶⁵ have recently introduced the concept of using noncovalently assembled liposomal SNAs, which, once in the cells, slowly release hydrophobically modified antisense oligonucleotides that could reach the nucleus and interact with the nucleic acids therein.

CONCLUSIONS

Novel polymer–oligonucleotide conjugates of comblike and coil-comb chain architectures were synthesized by grafting multiple single-stranded DNA oligonucleotide chains onto synthetic (co)polymers. An initiator-free azide-alkyne click reaction of dibenzocyclooctyne-functionalized ssODN and azido-functionalized (co)polymers – PN₃MS homopolymer as well as its random, P(N₃MS-*ran*-S), and block, PN₃MS-*b*-PS, copolymers with styrene – was employed to covalently attach 5–8 oligonucleotide strands per polymer chain. Given the distinct solubility of the polymer backbone and ssODN grafts in water, amphiphilic properties were conferred to the conjugates resulting in spontaneous formation of multichain nano-sized aggregates. They were relatively small in size (R_h in the 45–50 nm range) with moderately negative ζ potential (–15 – –18 mV range) as revealed by dynamic and electrophoretic light scattering, implying a core–shell structure that comprises a hydrophobic core built of the synthetic polymer and a shell of oligonucleotide strands. Further structural and compositional characterization of the new constructs was provided by SLS measurements. Information about the density of material within the particle, aggregation number, number of oligonucleotide strands per particle, and grafting density and how they depend on the chemical structure and composition of the conjugates was extracted and discussed. The novel constructs were found to carry thousands of DNA strands per particle at a grafting density approaching the grafting density at the transition to the brush regime implying unextended conformation of the strands. Although the brush regime was not reached, the oligonucleotide shell around the particles endowed the latter with hallmark biological properties of the SNAs: they were not toxic in a wide concentration range and exhibited enhanced nuclease stability (its relation with the grafting density was nicely demonstrated, particularly with the ssODNconjH aggregates) and rapid transfection agent-free cellular uptake in A549 cells. Developed and optimized with regard to general SNA features and introducing diversity in the synthetic approaches and tailorability in the composition, the present 3D nucleic acid nanostructures exhibit a set of valuable properties that make them promising materials with scope of utility in drug delivery, molecular diagnostics, and gene regulation as well as various nucleic acid-based therapeutic approaches.

ASSOCIATED CONTENT

Supporting Information

The Supporting Information is available free of charge at <https://pubs.acs.org/doi/10.1021/acs.biomac.3c00126>.

Composition and characterization of dibenzocyclooctyne-functionalized oligonucleotide – HPLC chromatogram and MALDI spectrum; synthesis, modification, and characterization of the polymer intermediates and polymer-oligonucleotide conjugates – reaction schemes, SEC chromatograms, ^1H NMR and UV spectra; determination of the average number of ssODN strands per (co)polymer chain; calculations of density of the material within the particle, grafting density, Flory radius, and grafting density at the transition from mushroom to brush conformation (PDF)

AUTHOR INFORMATION

Corresponding Authors

Natalia Toncheva-Moncheva – Institute of Polymers, Bulgarian Academy of Sciences, 1113 Sofia, Bulgaria; orcid.org/0000-0002-7257-1107; Email: ntoncheva@polymer.bas.bg

Stanislav Rangelov – Institute of Polymers, Bulgarian Academy of Sciences, 1113 Sofia, Bulgaria; Email: rangelov@polymer.bas.bg

Authors

Erik Dimitrov – Institute of Polymers, Bulgarian Academy of Sciences, 1113 Sofia, Bulgaria

Jordan A. Doumanov – Department of Biochemistry, Faculty of Biology, Sofia University "St. Kliment Ohridski" 8, 1164 Sofia, Bulgaria

Kirilka Mladenova – Department of Biochemistry, Faculty of Biology, Sofia University "St. Kliment Ohridski" 8, 1164 Sofia, Bulgaria

Svetla Petrova – Department of Biochemistry, Faculty of Biology, Sofia University "St. Kliment Ohridski" 8, 1164 Sofia, Bulgaria

Stergios Pispas – Theoretical and Physical Chemistry Institute, National Hellenic Research Foundation, 116 35 Athens, Greece; orcid.org/0000-0002-5347-7430

Complete contact information is available at:

<https://pubs.acs.org/10.1021/acs.biomac.3c00126>

Author Contributions

The manuscript was written through contributions of all authors. All authors have given approval to the final version of the manuscript.

Funding

This work was supported by the National Science Fund (Bulgaria) project no DN19/8-2017.

Notes

The authors declare no competing financial interest.

ACKNOWLEDGMENTS

Research equipment of Distributed Research Infrastructure INFRAMAT, part of the Bulgarian National Roadmap for Research Infrastructures, supported by the Bulgarian Ministry of Education and Science, was used in this investigation.

REFERENCES

- (1) Seeman, N. C. DNA in a Material World. *Nature* **2003**, *421*, 427–431.
- (2) Seeman, N. C. DNA Engineering and its Application to Nanotechnology. *Trends Biotechnol.* **1999**, *17*, 437–443.
- (3) Han, D.; Pal, S.; Nangreave, J.; Deng, Z.; Liu, Y.; Yan, H. DNA Origami with Complex Curvatures in Three-Dimensional Space. *Science* **2011**, *332*, 342–346.
- (4) Zhan, P.; Jahnke, K.; Liu, N.; Göpfrich, K. Functional DNA-Based Cytoskeletons for Synthetic Cells. *Nat. Chem.* **2022**, *14*, 958–963.
- (5) Seeman, N. C. An Overview of Structural DNA Nanotechnology. *Mol. Biotechnol.* **2007**, *37*, 246–257.
- (6) Chen, T.; Ren, L.; Liu, X.; Zhou, M.; Li, L.; Xu, J.; Zhu, X. DNA Nanotechnology for Cancer Diagnosis and Therapy. *Int. J. Mol. Sci.* **2018**, *19*, 1671.
- (7) Mokhtarzadeh, A.; Vahidnezhad, H.; Youssefian, L.; Mosafer, J.; Baradaran, B.; Uitto, J. Applications of Spherical Nucleic Acid Nanoparticles as Delivery Systems. *Trends Mol. Med.* **2019**, *25*, 1066–1079.
- (8) Cutler, J. I.; Auyeung, E.; Mirkin, C. A. Spherical Nucleic Acids. *J. Am. Chem. Soc.* **2012**, *134*, 1376–1391.
- (9) Hao, L.; Patel, P. C.; Alhasan, A. H.; Giljohann, D. A.; Mirkin, C. A. Nucleic Acid–Gold Nanoparticle Conjugates as Mimics of MicroRNA. *Small* **2011**, *7*, 3158–3162.
- (10) Bakardzhiev, P.; Toncheva-Moncheva, N.; Mladenova, K.; Petrova, S.; Videv, P.; Moskova-Doumanova, V.; Topouzova-Hristova, T.; Doumanov, J.; Rangelov, S. Assembly of Amphiphilic Nucleic Acid–Polymer Conjugates into Complex Superaggregates: Preparation, Properties, and in vitro Performance. *Eur. Polym. J.* **2020**, *131*, 109692.
- (11) Kapadia, C. H.; Melamed, J. R.; Day, E. S. Spherical Nucleic Acid Nanoparticles: Therapeutic Potential. *BioDrugs* **2018**, *32*, 297–309.
- (12) Guan, C.; Chernyak, N.; Dominguez, D.; Cole, L.; Zhang, B.; Mirkin, C. A. RNA-Based Immunostimulatory Liposomal Spherical Nucleic Acids as Potent TLR7/8 Modulators. *Small* **2018**, *14*, No. e1803284.
- (13) Teplensky, M. H.; Distler, M. E.; Kusmierz, C. D.; Evangelopoulos, M.; Gula, H.; Elli, D.; Tomatsidou, A.; Nicolaescu, V.; Gelarden, I.; Yeldandi, A.; Battle, D.; Missiakas, D.; Mirkin, C. A. Spherical Nucleic Acids as an Infectious Disease Vaccine Platform. *PNAS* **2022**, *119*, No. e2119093119.
- (14) Xiao, F.; Lin, L.; Chao, Z.; Shao, C.; Chen, Z.; Wei, Z.; Lu, J.; Huang, Y.; Li, L.; Liu, Q.; Liang, Y.; Tian, L. Organic Spherical Nucleic Acids for the Transport of a NIR-II-Emitting Dye Across the Blood–Brain Barrier. *Angew. Chem., Int. Ed.* **2020**, *59*, 9702–9710.
- (15) Bousmail, D.; Amrein, L.; Fakhoury, J. J.; Fakhir, H. H.; Hsu, J. C. C.; Panasci, L.; Sleiman, H. F. Precision Spherical Nucleic Acids for Delivery of Anticancer Drugs. *Chem. Sci.* **2017**, *8*, 6218–6229.
- (16) Briley, W.; Halo, T. L.; Randeria, P. S.; Alhasan, A. H.; Auyeung, E.; Hurst, S. J.; Mirkin, C. A. Biochemistry and Biomedical Applications of Spherical Nucleic Acids (SNAs). In *Nanomaterials for Biomedicine*; Nagarajan, R., Ed.; ACS Symposium Series; American Chemical Society: Washington, DC, 2012; p 1–20.
- (17) Giljohann, D. A.; Seferos, D. S.; Daniel, W. L.; Massich, M. D.; Patel, P. C.; Mirkin, C. A. Gold Nanoparticles for Biology and Medicine. *Angew. Chem., Int. Ed.* **2010**, *49*, 3280–3294.
- (18) Sandhu, K. K.; McIntosh, C. M.; Simard, J. M.; Smith, S. W.; Rotello, V. M. Gold Nanoparticle-Mediated Transfection of Mammalian Cells. *Bioconjugate Chem.* **2002**, *13*, 3–6.
- (19) Kumar, M. N. V.; Sameti, M.; Mohapatra, S. S.; Kong, X.; Lockey, R. F.; Bakowsky, U.; Lindenblatt, G.; Schmidt, C. H.; Lehr, C.-M. Cationic Silica Nanoparticles as Gene Carriers: Synthesis, Characterization and Transfection Efficiency *in vitro* and *in vivo*. *J. Nanosci. Nanotechnol.* **2004**, *4*, 876–881.
- (20) Rosi, N. L.; Giljohann, D. A.; Thaxton, C. S.; Lytton-Jean, A. K. R.; Han, M. S.; Mirkin, C. A. Oligonucleotide-Modified Gold Nanoparticles for Intracellular Gene Regulation. *Science* **2006**, *312*, 1027–1030.
- (21) Giljohann, D. A.; Seferos, D. S.; Progodich, A. E.; Patel, P. C.; Mirkin, C. A. Gene Regulation with Polyvalent siRNA-Nanoparticle Conjugates. *J. Am. Chem. Soc.* **2009**, *131*, 2072–2073.

- (22) Davis, M. E.; Chen, Z.; Shin, D. M. Nanoparticle Therapeutics: an Emerging Treatment Modality for Cancer. *Nat. Rev. Drug. Discovery* **2008**, *7*, 771–782.
- (23) Dobson, J. Gene Therapy Progress and Prospects: Magnetic Nanoparticle-Based Gene Delivery. *Gene Ther.* **2006**, *13*, 283–287.
- (24) Song, Y.; Song, W.; Lan, X.; Cai, W.; Jiang, D. Spherical Nucleic Acids: Organized Nucleotide Aggregates as Versatile Nanomedicine. *Aggregate* **2022**, *3*, No. e120.
- (25) Lee, J. S.; Lytton-Jean, A. K. R.; Hurst, S. J.; Mirkin, C. A. Silver Nanoparticle-Oligonucleotide Conjugates Based on DNA with Triple Cyclic Disulfide Moieties. *Nano Lett.* **2007**, *7*, 2112–2115.
- (26) Cutler, J. I.; Zheng, D.; Xu, X.; Giljohann, D. A.; Mirkin, C. A. Polyvalent Oligonucleotide Iron Oxide Nanoparticle “Click” Conjugates. *Nano Lett.* **2010**, *10*, 1477–1480.
- (27) Dimitrov, E.; Toncheva-Moncheva, N.; Bakardzhiev, P.; Forsys, A.; Dumanov, J.; Mladenova, K.; Petrova, S.; Trzebicka, B.; Rangelov, S. Original Synthesis of a Nucleolipid for Preparation of Vesicular Spherical Nucleic Acids. *Nanomaterials* **2022**, *12*, 3645.
- (28) Haladjova, E.; Petrova, M.; Ugrinova, I.; Forsys, A.; Trzebicka, B.; Rangelov, S. Hollow Spherical Nucleic Acid Structures Based on Polymer-Coated Phospholipid Vesicles. *Soft Matter* **2022**, *18*, 5426–5434.
- (29) Zhang, C.; Hao, L.; Calabrese, C. M.; Zhou, Y.; Choi, C. H. J.; Xing, H.; Mirkin, C. A. Biodegradable DNA-Brush Block Copolymer Spherical Nucleic Acids Enable Transfection Agent-Free Intracellular Gene Regulation. *Small* **2015**, *11*, 5360–5368.
- (30) Lee, S. H.; Mok, H.; Lee, Y.; Park, T. G. Self-Assembled siRNA–PLGA Conjugate Micelles for Gene Silencing. *J. Controlled Release* **2011**, *152*, 152–158.
- (31) Teixeira, F., Jr.; Rigler, P.; Vebert-Nardin, C. Nucleo-Copolymers: Oligonucleotide-Based Amphiphilic Diblock Copolymers. *Chem. Commun.* **2007**, *11*, 1130–1132.
- (32) Kim, C.-J.; Jeong, E. H.; Lee, H.; Park, S.-J. A Dynamic DNA Nanostructure with Switchable and Size-Selective Molecular Recognition Properties. *Nanoscale* **2019**, *11*, 2501–2509.
- (33) Vlassi, E.; Pispas, S. Imidazolium Quaternized Polymers Based On Poly(Chloromethyl Styrene) and their Complexes with FBS Proteins and DNA. *Macromol. Chem. Phys.* **2015**, *216*, 1718–1728.
- (34) Provencher, S. W. Inverse Problems in Polymer Characterization: Direct Analysis of Polydispersity with Photon Correlation Spectroscopy. *Makromol. Chem.* **1979**, *180*, 201–209.
- (35) Moad, G.; Rizzardo, E. Chapter 1: The History of Nitroxide-mediated Polymerization. In *Nitroxide Mediated Polymerization: From Fundamentals to Applications in Materials Science*; Gígenes, D., Ed.; Polymer Chemistry Series; Royal Society of Chemistry, 2015; p 1.
- (36) Burchard, W. Static and Dynamic Light Scattering from Branched Polymers and Biopolymers. In *Light Scattering from Polymers*; Advances in Polymer Science, Springer: Berlin, Heidelberg, 1983; Vol. 48, p. 1.
- (37) Thurn, A.; Burchard, W.; Niki, R. Structure of Casein Micelles I. Small Angle Neutron Scattering and Light Scattering from β - and γ -Casein. *Colloid Polym. Sci.* **1987**, *265*, 653–666.
- (38) Burchard, W. *Light Scattering: Principles and Development*; Brown, W., Ed.; Clarendon Press: Oxford, 1996, p 439.
- (39) Johnsson, M.; Hansson, P.; Edwards, K. Spherical Micelles and Other Self-Assembled Structures in Dilute Aqueous Mixtures of Poly(Ethylene Glycol) Lipids. *J. Phys. Chem. B* **2001**, *105*, 8420–8430.
- (40) Rangelov, S.; Almgren, M.; Tsvetanov, C.; Edwards, K. Shear-Induced Rearrangement of Self-Assembled PEG-Lipids Structures in Water. *Macromolecules* **2002**, *35*, 7074–7081.
- (41) Bakardzhiev, P.; Rangelov, S.; Trzebicka, B.; Momekova, D.; Lalev, G.; Garamus, V. M. Nanostructures by Self-Assembly of Polyglycidol-Derivatized Lipids. *RSC Adv.* **2014**, *4*, 37208–37219.
- (42) Wanka, G.; Hoffmann, H.; Ulbricht, W. Phase Diagrams and Aggregation Behavior of Poly(oxyethylene)-Poly(oxypropylene)-Poly(oxyethylene) Triblock Copolymers in Aqueous Solutions. *Macromolecules* **1994**, *27*, 4145–4159.
- (43) Yu, G.-E.; Garrett, C. A.; Mai, S.-M.; Altinok, H.; Attwood, D.; Price, C.; Booth, C. Effect of Cyclization on the Association Behavior of Block Copolymers in Aqueous Solution. Comparison of Oxyethylene/Oxypropylene Block Copolymers Cyclo-P₃₄E₁₀₄ and E₅₂P₃₄E₅₂. *Langmuir* **1998**, *14*, 2278–2285.
- (44) Taton, T. A.; Mirkin, C. A.; Letsinger, R. L. Scanometric DNA Array Detection with Nanoparticle Probes. *Science* **2000**, *289*, 1757–1760.
- (45) Li, Z.; Zhang, Y.; Fullhart, P.; Mirkin, C. A. Reversible and Chemically Programmable Micelle Assembly with DNA Block-Copolymer Amphiphiles. *Nano Lett.* **2004**, *4*, 1055–1058.
- (46) Calabrese, C. M.; Merkel, T. J.; Briley, W. E.; Randeria, P. S.; Narayan, S. P.; Rouge, J. L.; Walker, D. A.; Scott, A. W.; Mirkin, C. A. Biocompatible Infinite-Coordination-Polymer Nanoparticle-Nucleic Acid Conjugates for Antisense Gene Regulation. *Angew. Chem., Int. Ed.* **2015**, *54*, 476–480.
- (47) Hurst, S. J.; Lytton-Jean, A. K. R.; Mirkin, C. A. Maximizing DNA Loading on a Range of Gold Nanoparticle Sizes. *Anal. Chem.* **2006**, *78*, 8313–8318.
- (48) Haladjova, E.; Ugrinova, I.; Rangelov, S. One-Pot Synthesis of Oligonucleotide-Grafted Polymeric Nanoparticles. *Soft Matter* **2020**, *16*, 191–199.
- (49) Dimitrov, E.; Toncheva-Moncheva, N.; Bakardzhiev, P.; Forsys, A.; Dumanov, J.; Mladenova, K.; Petrova, S.; Trzebicka, B.; Rangelov, S. Nucleic Acid-Based Supramolecular Structures: Vesicular Spherical Nucleic Acids from a Non-Phospholipid Nucleolipid. *Nanoscale Adv.* **2022**, 3793–3803.
- (50) Banga, R. J.; Krovi, S. A.; Narayan, S. P.; Sprangers, A. J.; Liu, G.; Mirkin, C. A.; Nguyen, S. T. Drug-Loaded Polymeric Spherical Nucleic Acids: Enhancing Colloidal Stability and Cellular Uptake of Polymeric Nanoparticles through DNA Surface Functionalization. *Biomacromolecules* **2017**, *18*, 483–489.
- (51) Banga, R. J.; Chernyak, N.; Narayan, S. P.; Nguyen, S. T.; Mirkin, C. A. Liposomal Spherical Nucleic Acids. *J. Am. Chem. Soc.* **2014**, *136*, 9866–9869.
- (52) Flory, P. J. *Principles of Polymer Chemistry*; Cornell University Press: Ithaca, NY, 1953.
- (53) Tancini, B.; Buratta, S.; Delo, F.; Sagini, K.; Chiaradia, E.; Pellegrino, R. M.; Emiliani, C.; Urbanelli, L. Lysosomal Exocytosis: The Extracellular Role of an Intracellular Organelle. *Membranes* **2020**, *10*, 406.
- (54) Patel, P. C.; Giljohann, D. A.; Daniel, W. L.; Zheng, D.; Prigodich, A. E.; Mirkin, C. A. Scavenger Receptors Mediate Cellular Uptake of Polyvalent Oligonucleotide-Functionalized Gold Nanoparticles. *Bioconjugate Chem.* **2010**, *21*, 2250–2256.
- (55) Fukasawa, M.; Adachi, H.; Hirota, K.; Tsujimoto, M.; Arai, H.; Inoue, K. SRB1, a Class B Scavenger Receptor, Recognizes both Negatively Charged Liposomes and Apoptotic Cells. *Exp. Cell Res.* **1996**, *222*, 246–250.
- (56) Sakurai, F.; Nishioka, T.; Saito, H.; Baba, T.; Okuda, A.; Matsumoto, O.; Taga, T.; Yamashita, F.; Takakura, Y.; Hashida, M. Interaction between DNA–Cationic Liposome Complexes and Erythrocytes is an Important Factor in Systemic Gene Transfer via the Intravenous Route in Mice: the Role of the Neutral Helper Lipid. *Gene Ther.* **2001**, *8*, 677–686.
- (57) Poojari, C.; Wilkosz, N.; Lira, R. B.; Dimova, R.; Jurkiewicz, P.; Petka, R.; Kepczynski, M.; Róg, T. Behavior of the DPH Fluorescence Probe in Membranes Perturbed by Drugs. *Chem. Phys. Lipids* **2019**, *223*, 104784.
- (58) Lakowicz, J. R. *Principles of Fluorescent Spectroscopy*; Springer Science+Business Media: New York, NY, 1983; p. 72.
- (59) Haugland, R. P. *Handbook of Fluorescent Probes and Research Chemicals*; Eugene, O. R., Ed.; Molecular Probes Inc.: Eugene, OR, 1992.
- (60) Genz, A.; Holzwarth, J. F. Dynamic Fluorescence Measurements on the Main Phase Transition of Dipalmytoylphosphatidylcholine Vesicles. *Eur. Biophys. J.* **1986**, *13*, 323–330.
- (61) Alexandridis, P.; Holzwarth, J. F.; Hatton, T. A. Micellization of Poly(ethylene oxide)-Poly(propylene oxide)-Poly(ethylene oxide)

Triblock Copolymers in Aqueous Solutions: Thermodynamics of Copolymer Association. *Macromolecules* **1994**, *27*, 2414–2425.

(62) Scherlund, M.; Brodin, A.; Malmsten, M. Micellization and Gelation in Block Copolymer Systems Containing Local Anesthetics. *Int. J. Pharm.* **2000**, *211*, 37–49.

(63) Halacheva, S.; Rangelov, S.; Tsvetanov, C.; Garamus, V. M. Aqueous Solution Properties of Polyglycidol-based Analogues of Pluronic Copolymers. Influence of the Poly(propylene oxide) Block Molar Mass. *Macromolecules* **2010**, *43*, 772–781.

(64) Behzadi, S.; Serpooshan, V.; Tao, W.; Hamaly, M. A.; Alkawareek, M. Y.; Dreadene, E. C.; Brown, D.; Alkilany, A. M.; Farokhzad, O. C.; Mahmoudi, M. Cellular Uptake of Nanoparticles: Journey Inside the Cell. *Chem. Soc. Rev.* **2017**, *46*, 4218–4244.

(65) Sprangers, A. J.; Hao, L.; Banga, R. J.; Mirkin, C. A. Liposomal Spherical Nucleic Acids for Regulating Long Noncoding RNAs in the Nucleus. *Small* **2017**, *13*, 1602753.

Recommended by ACS

Customized Scaffolds for Direct Assembly of Functionalized DNA Origami

Esra Oktay, Remi Veneziano, *et al.*

JUNE 02, 2023

ACS APPLIED MATERIALS & INTERFACES

READ 

Stabilizing Polymer Coatings Alter the Protein Corona of DNA Origami and Can Be Engineered to Bias the Cellular Uptake

Hugo J. Rodríguez-Franco, Maartje M. C. Bastings, *et al.*

JUNE 07, 2023

ACS POLYMERS AU

READ 

Sulfonium-Driven Neoantigen-Released DNA Nanodevice as a Precise Vaccine for Tumor Immunotherapy and Prevention

Yaping Zhang, Zigang Li, *et al.*

NOVEMBER 01, 2022

ACS NANO

READ 

Block Copolymer Micellization of DNA Origami Promotes Solubility in Organic Solvents

Nayan P. Agarwal, Thorsten L. Schmidt, *et al.*

SEPTEMBER 14, 2022

LANGMUIR

READ 

Get More Suggestions >